Critical pressure values for graphene membrane covering a slit

Alexander V. Savin[1,2,*] and Sergey V. Dmitriev[3,4,†]

[1]*N.N. Semenov Federal Research Center for Chemical Physics of the Russian Academy of Sciences, 4 Kosygin St., Moscow 119991, Russia*
[2]*Plekhanov Russian University of Economics, 36 Stremyanny Lane, Moscow 117997, Russia*
[3]*Institute of Molecule and Crystal Physics, UFRC of Russian Academy of Sciences, Oktyabrya Ave. 151, Ufa 450075, Russia*
[4]*Polytechnic Institute (Branch) in Mirny, North-Eastern Federal University, Tikhonova St. 5/1, 678170 Mirny, Sakha Republic (Yakutia), Russia*

(Received 13 May 2023; revised 12 September 2023; accepted 13 September 2023; published 17 October 2023)

Graphene is impervious to gases, so the question arises of how much pressure can few-layer graphene covering a slit withstand. Using the molecular dynamics model with a reduced number of degrees of freedom, a multilayer graphene sheet lying on an h-BN substrate with a slit of width d is considered under external or internal pressure p. It has been established that at $p < p_0$, where p_0 is the critical pressure, a graphene sheet under pressure acquires a stationary profile and seals the slit. At $p > p_0$, the graphene sheet loses its connection with the substrate and the ability to seal the slit. The critical pressure is almost proportional to $1/d$ and decreases linearly with increasing temperature. An increase in the number of graphene layers in a graphene sheet slightly reduces p_0 only at $d < 10$ nm, and for wider slits, the number of graphene layers does not affect p_0. This fact is explained by the membrane theory. The graphene sheet can seal the atmospheric pressure for a slit with a width of no more than 0.01 mm. Presented results are of interest for nanotechnologies using graphene membranes as sensors or resonators.

DOI: 10.1103/PhysRevB.108.144107

I. INTRODUCTION

Layered two-dimensional (2D) materials such as graphene (G) and hexagonal boron nitride (h-BN) are attracting great interest from researchers due to their unique electronic [1–3] and mechanical [4–7] properties. Graphene has a record high tensile Young's modulus (1 TPa) and strength (50–60 GPa) [8–11], a very high melting point (5000 K) [12], thermal conductivity [13–15], and is chemically stable in the absence of oxidizers [16–18]. To describe the mechanical properties of multilayer nanomaterials, theoretical models are being developed [19–21].

Currently, heterogeneous layered materials, which can exhibit various new mechanical and physical properties compared to their homogeneous counterparts [22–25], are of increased interest. For example, the use of G/h-BN heterostructures makes it possible to obtain the desired electronic properties [26,27], as well as to significantly reduce the friction [28,29] between layers [30]. Boron nitride is an attractive substrate for graphene because it has an atomically smooth surface free of dangling bonds, a lattice constant similar to that of graphite, and a large band gap [31–33]. Van der Waals and covalent interactions in a vertical heterostructure composed of boron and carbon were analyzed in the work [34]. Nontrivial mechanical properties of structural metamaterials were reported in Refs. [35–38].

Dislocations and ripplocations in layered van der Waals materials were studied using analytical and computational techniques to demonstrate that the ripplocation is the lowest-energy structure of dislocation pileups, while large dislocation pileups in bulk graphite demonstrate multilayer delamination and voids [39]. Formation of ripplocations is a deformation mechanism of multilayer graphene [40–42]. Dynamics and collisions of surface ripplocations were analyzed numerically in Ref. [43].

Using atomic force microscopy, mechanical folding in uniaxially compressed single-layer graphene on a substrate was studied, and various mechanisms of stress release during delamination and folding were described [44].

Pressurized blister tests are used to measure the adhesion energy of graphene sheets with a substrate and other mechanical properties of layered materials [41,45,46].

The bending stiffness of circular multilayer van der Waals material sheets under bulge tests can demonstrate relatively high values [47]. The importance of taking into account thermal fluctuations for modeling the mechanical properties of multilayer graphene was demonstrated in Ref. [48]. Graphene nanoribbons are supersoft in bending; they can slide over each other, bend, filling in the unevenness of the substrate [7]. 2D materials are actually not perfectly flat as they have wrinkles, blisters, and other imperfections [49–52].

In a series of works [53–55], a theoretical model has been developed to account for the effect of temperature on decohesion and fracture at the micro- and nanoscale. The mechanical model describes a chain interacting with a substrate through a series of bonds that can be either breakable or bistable. The pulling process can be initiated by an applied force or controlled by a prescribed displacement at the end of the chain. The model has been solved exactly to characterize the

*asavin00@gmail.com
†dmitriev.sergey.v@gmail.com

critical temperature corresponding to the complete detachment of the chain in the fragile or ductile regime.

Very often, 2D materials suspended above a trench or a round hole are considered as nanomechanical resonators promising for biological and chemical detection and measurement of ultralow masses and accelerations [56–58]. Similar configurations are used as sensors [19] and to measure the mechanical properties of two-dimensional materials and their interaction with the substrate, friction, and adhesion. The progress in the development of experimental techniques of contact probing of mechanical, interfacial, and tribological properties of 2D materials is summarized in the review [59].

A molecular dynamics simulation of a graphene sheet suspended above a trench was carried out to study the effect of self-tensioning in the sheet [60]. It was shown that the depth in the middle of the sheet does not depend on the width of the trench and is proportional to the temperature and the strength of the interaction of graphene with the substrate. Heating (cooling) of a graphene sheet was observed during molecular dynamics simulation of the stamping (peeling) process on (off) the (111) surface of a Pt substrate [61]. In Ref. [62], a method was proposed to measure the stiffness of a nanosheet using indentation or bulge tests. The authors took into account such difficulties as slippage, pretensioning, and substrate roughness. Thin film peeling was modeled in Ref. [63] taking into account possible contact of the film with a rough rigid surface. Rich dynamics in peeling and sliding of graphene nanoribbons atop a graphite substrate was studied numerically by a continuum model [64]. A cylindrical chamber in SiO_2 substrate sealed with a few-layer graphene under external pressure was used to study friction at the interface [65]. The mechanics of droplets covered with elastic membranes was analyzed in the work [66], where bubble pressure and interfacial energies were estimated.

Graphene is considered impermeable to all gases including helium [67–69], except hydrogen [70]. This allows us to produce from graphene molecular valves [71] or semipermeable membranes by artificially making angstrom-sized holes [72,73] or using natural pores in grain boundaries [74].

In this work, the possibility of sealing nano- and microcracks with few-layer graphene sheets is analyzed. The simulation setup is described in Sec. II, the numerical results are presented in Sec. III, and the results of continuum mechanics treatment in Sec. IV. Section V concludes our work.

II. SIMULATIONS SETUP

First, 3D model is analyzed and then the chain model is described, which allows one to reduce the considered full-atomic model to a 2D problem. Then methods for finding the ground state of the structure and taken into account the influence of temperature and pressure are described.

A. 3D model

Consider a rectangular (square) single-layer graphene sheet of size 18.05×18.15 nm^2 (the number of carbon atoms is $N_C = 12726$) on a two-layer substrate of h-BN. Let us take a square substrate of size 20.76×20.69 nm^2 and make a rectangular hole of size $d_x\times d_y$ ($d_x = 6.14$ nm, $d_y = 6.22$, 12.01, and 18.09 nm) in its center. The graphene sheet is symmetrically centered on the substrate, see Fig. 1 (the zigzag direction of the sheet and the substrate coincides with the x axis). As a result, the rectangular central part of the graphene sheet is suspended, forming a single-layer rectangular membrane. Let us consider the dynamics of this membrane under the action of an external or internal pressure p.

The atoms of the substrate are considered stationary (fixed at their lattice positions), and the dynamics of the graphene sheet is modeled by the method of molecular dynamics using the Langevin thermostat. The Hamiltonian of the graphene sheet is

$$H = \sum_{n=1}^{N_C}\left[\frac{1}{2}M_n(\dot{\mathbf{u}}_n,\dot{\mathbf{u}}_n) + E_n + P(\mathbf{u}_n)\right], \tag{1}$$

where the vector $\mathbf{u}_n = (x_n, y_n, z_n)$ defines the coordinates of the nth carbon atom and the overdot means differentiation with respect to time.

The first summand in Eq. (1) defines the kinetic energy. It is assumed that hydrogen atoms are attached to the edge atoms of the graphene sheet, so the masses of the inner atoms are $M_n = 12m_p$ and of the edge atoms are $M_n = 13m_p$ (m_p is the mass of a proton). The second summand, E_n, sets the interaction energy of the nth atom with neighboring carbon atoms. Here the deformations of valence bonds, valence, and dihedral (torsional) angles are taken into account; a detailed description of the force field used is given in Ref. [75]. The last summand, $P(\mathbf{u}_n)$, describes the energy of nonvalent interaction of the carbon atoms with the h-BN substrate atoms:

$$P(\mathbf{u}_n) = \sum_{k=1}^{N_s} W_i(r_{n,k}),$$

where N_s is the number of atoms in the substrate, $r_{n,k}$ is the distance from nth carbon atom to kth substrate atom. The nonvalent interactions are described by the Lennard-Jones potential,

$$W_i(r) = \varepsilon_i(r_i/r)^6[(r_i/r)^6 - 2], \quad i = 1, 2,$$

where for a pair of interacting atoms C, N $\varepsilon_i = 0.00369$ eV, $r_i = 3.756$ Å ($i = 1$); for a pair C, B $\varepsilon_i = 0.00596$ eV, $r_i = 3.967$ Å ($i = 2$) [76].

The dynamics of the nanoribbon is described by a system of Langevin equations

$$M_n\ddot{\mathbf{u}}_n = -\frac{\partial H}{\partial \mathbf{u}_n} - \Gamma M_n\dot{\mathbf{u}}_n + \Xi_n + \mathbf{f}_n, \quad n = 1,\ldots,N_C, \tag{2}$$

where $\Gamma = 1/t_r$ is the friction coefficient characterizing the intensity of energy exchange with the thermostat (relaxation time $t_r = 1$ ps), $\Xi_n = \{\xi_{n,i}\}_{i=1}^3$ is the three-dimensional vector of normally distributed random forces normalized by the following conditions:

$$\langle\xi_{n,i}(t)\xi_{k,j}(s)\rangle = 2M_nk_BT\Gamma\delta_{nk}\delta_{ij}\delta(s-t),$$

where T is the thermostat temperature, k_B is the Boltzmann constant. The vector $\mathbf{f}_n$ in Eq. (2) models a constant pressure acting orthogonally to the surface of the sheet. The pressure force is assumed to act on the center of gravity of each valence hexagon orthogonal to its plane, and the magnitude of the

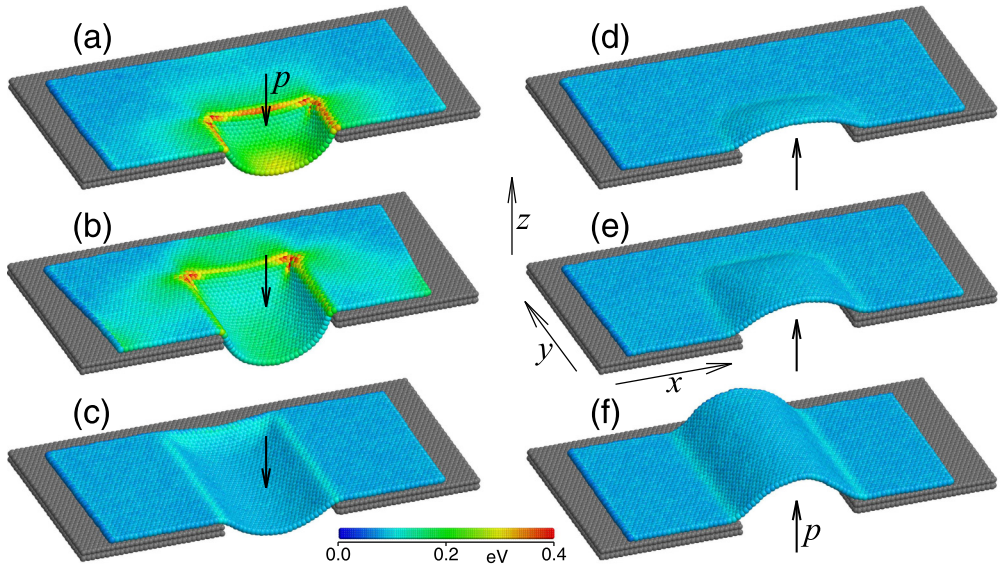

FIG. 1. Stationary configurations of a single-layer square graphene membrane on the *h*-BN substrate with a rectangular hole under the pressure p slightly below the critical value p_0: (a)–(c) external pressure, (d)–(f) internal pressure. The size of the graphene sheet is 18.05×18.15 nm^2, while a two-layer *h*-BN substrate, shown in gray, has a size of 20.76×20.15 nm^2. A hole in the center of the substrate has a size of (a), (d) 6.14×6.22, (b), (e) 6.14×12.01, and (c), (f) 6.14×18.09 nm^2. The zigzag direction of the graphene sheet and the substrate coincides with the x axis. The atoms of the substrate are fixed in their lattice positions and only the atoms of the graphene sheet can move. In (a)–(c), the external pressure is $p = 41$, 17.5, and 2.1 eV/nm^3, respectively. In (d)–(f) the internal pressure is $p = 4.6$, 3.0, and 1.4 eV/nm^3, respectively. Temperature $T = 300$ K. For simplicity, only half of the system ($y > 0$) is shown, since the other half looks similar due to symmetry. The atoms of graphene are colored according to their energy, as indicated by the color bar.

force is directly proportional to the hexagon area (this force is distributed equally over the six atoms forming the hexagon). When modeling the external pressure (from above), the force $\mathbf{f}_n$ is applied to all hexagons. When modeling the internal pressure acting from the hole in the substrate, the force is applied only to hexagons not adjacent to the substrate. As the pressure pulls the sheet away from the substrate, see Figs. 1(d)–1(f), the number of hexagons on which the pressure acts also increases.

In our simulations, the pressure is applied quasistatically to avoid the effect of viscous friction between the graphene and the substrate.

The equations of motion Eq. (2) are solved numerically using the fourth-order Verlet method [77]. A time step of 1 fs is used in the simulations, since further reduction of the time step has no appreciable effect on the results.

Numerical modeling has shown that the graphene sheet can withstand pressure only up to a critical value p_0, which depends on the shape and size of the hole in the substrate. When $p < p_0$, the sheet bends in the hole region under the action of pressure. A deformed steady state of the sheet is formed in which the pressure is compensated by the sheet deformation forces. As the pressure $p < p_0$ increases, the sheet deformation increases. When the critical value of external pressure, $p = p_0$, is reached, either the sheet breaks or it is pulled through the hole in the substrate. At critical internal pressure, the sheet detaches from the substrate.

Under the action of external pressure, the sheet is pressed into the hole of the substrate–see Figs. 1(a)–1(c). The deformation scenario depends on the shape of the hole. If the hole is square, the deformation occurs symmetrically due to stretching of the valence bonds. The largest bond deformations occur along the perimeter of the hole, see Fig. 1(a). Here, valence bond rupture occurs when the critical pressure value is reached. Such a scenario of graphene membrane rupture under pressure was previously found for holes with the shape of a circle [78] and a regular hexagon [79].

The sheet deformation scenario changes with increasing hole asymmetry. A twofold increase in the length of the rectangular hole, see Fig. 1(b), causes the sheet to be pushed into the hole, accompanied by sliding of the sheet edges on the substrate. As a result, at a critical pressure, valence bond rupture does not occur and the entire sheet is squeezed through the hole in a crumpled form. If the hole length is increased by a factor of three, see Fig. 1(c), the sheet width becomes only slightly larger than the hole length. In this case, the sheet is pressed into the hole without significant stretching of the valence bonds, only by the bending and sliding of the sheet on the substrate. The main resistance to pressure is provided by the nonvalence interactions between the sheet and the substrate.

Under the action of internal pressure, the sheet deformation scenario does not depend on the shape and size of the hole. At pressures below the critical value $p < p_0$, the valence bonds deform weakly and the sheet takes the shape of a bubble, see Figs. 1(d)–1(f). At $p = p_0$, the bubble starts to grow dynamically, causing the sheet to detach completely from the substrate. Here, the resistance to pressure is only due to weak nonvalent interactions between the graphene sheet and the substrate. Experiments on graphene sheet detachment due to internal pressure allow us to estimate the adhesion energy of the sheet to the substrate [80].

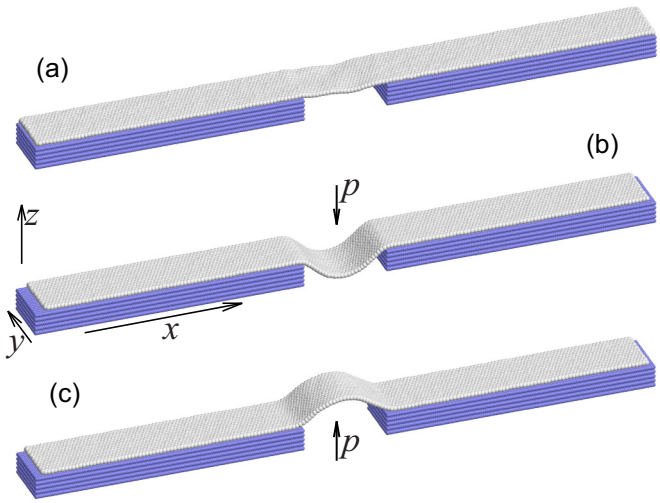

FIG. 2. The stationary configurations of a single-layer graphene membrane covering a straight slit of width $d = 6$ nm in a five-layer h-BN substrate. The periodic boundary condition with period $\Delta y = 8a_y \approx 3.403$ nm, is used along the y axis. The nanoribbon length is $L = 176a_x = 43.08$ nm, the number of carbon atoms is $N_C = 5632$. In (a) there is no pressure, $p = 0$, in (b) the external pressure is $p = 1.24$ eV/nm^3, and in (c) the internal pressure is $p = 0.92$ eV/nm^3 (these values are slightly below the critical value p_0). Temperature $T = 300$ K.

If the hole has the shape of an elongated rectangle, then the bubble has an elongated form, see Figs. 1(c), 1(f). To model the graphene sheet above an infinitely long straight slit in the substrate, it is convenient to use periodic boundary conditions along the y axis for the graphene sheet and the substrate. The graphene sheet has the zigzag direction along the x axis, then the armchair direction is along the y axis. The longitudinal lattice spacing of graphene is $a_x = \sqrt{3}r_0 = 2.456$ Å and the transverse is $a_y = 3r_0 = 4.254$ Å, where $r_0 = 1.418$ Å is the length of the C-C valence bond.

To model the graphene sheet above the infinite slit, a zigzag graphene nanoribbon of length $L = N_x a_x$ and width $\Delta y = N_y a_y$ is used, where N_x and N_y are integers. The nanoribbon consists of $N_C = 4N_x N_y$ carbon atoms. The nanoribbon length is fixed, $L = 176a_x = 43.08$ nm, while different values of the nanoribbon width are considered. Consider $N_y = 1, 2, 4, 8, 16$, and 32 (nanoribbon widths $\Delta y = 0.425$, 0.851, 1.702, 3.403, 6.806, and 13.613 nm). A five-layer h-BN substrate with a slit of width $d = 6$ nm in the center is considered, see Fig. 2(a).

Modeling of the sheet dynamics showed that under the external pressure, the sheet is always pressed into the slit due to its sliding on the substrate, see Fig. 2(b). The graphene nanoribbon slides on the substrate freely, with almost zero traction force. The bending amplitude of the nanoribbon increases monotonically with increasing pressure. When the critical pressure value p_0 is reached, the stationary deformation of the nanoribbon changes to the dynamic pressing into the slit.

Under the internal pressure, the nanoribbon forms a bubble above the slit due to sliding on the substrate, see Fig. 2(c). The height of the stationary bubble increases monotonically with increasing pressure p. When the critical value p_0 is reached, the nanoribbon is dynamically detached from the substrate.

TABLE I. The dependence of the critical external ($p_{0,1}$) and internal ($p_{0,2}$) pressure on the nanoribbon width Δy. The width of the slit in the substrate is $d = 6$ nm.

N_y	Δy (Å)	$p_{0,1}$ (eV/nm^3)	$p_{0,2}$ (eV/nm^3)
1	4.25	1.14	0.88
2	8.51	1.24	0.90
4	17.02	1.24	0.92
8	34.03	1.24	0.92
16	68.06	1.25	0.93
32	136.1	1.25	0.93

Note that the stationary form of the nanoribbon above the slit has a cross section that does not depend on the coordinate y; this indicates that the plane strain conditions are realized. Table I shows the dependence of the critical pressure $p_{0,i}$ ($i = 1$ for external and $i = 2$ for internal pressure) on the nanoribbon width Δy. As can be seen from the table, the critical pressure changes very little (about 10%) and saturates rapidly with increasing nanoribbon width.

In the following, the dynamics of a graphene sheet covering an infinitely long slit in the h-BN substrate is analyzed using a two-dimensional model shown in Fig. 3. In this case, the bending of the graphene sheet is modeled under the assumption of the plane strain condition, which was justified by considering the 3D model. In the two-dimensional model, the number of degrees of freedom is significantly reduced, which allows us to simulate multilayer membranes of large dimensions, taking into account the mobility of the substrate. Despite significant simplifications, the two-dimensional model correctly describes the behavior of multilayer membranes and provides realistic estimates for critical pressure values.

B. 2D model

In this study, a layered structure from nanoribbons of graphene (G) and hexagonal boron nitride (h-BN) is considered under internal or external pressure p, see Fig. 3. It is

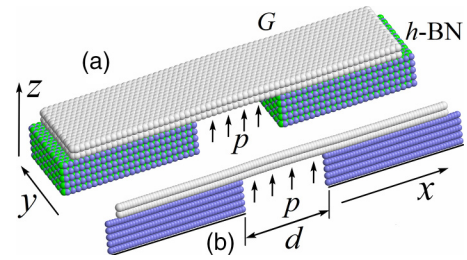

FIG. 3. Scheme for constructing a two-dimensional chain model for a bilayer graphene (G) sheet lying on a flat surface of a boron nitride (h-BN) crystal with a slit of width $d = 4$ nm under internal pressure p. The zigzag direction of all nanoribbons is along the x axis. The number of sheets in the substrate is $K_1 = 5$ and in G sheet $K_2 = 2$. In (a) the full-atomic 3D model is shown, and in (b) its 2D reduction is presented. Each node of the 2D model represents the movement of atoms in a rigid chain parallel to the y axis and having two degrees of freedom, coordinates (x, z).

assumed that the plane strain conditions are satisfied and the 3D full-atomic model shown in Fig. 3(a) is replaced by a 2D model of molecular chains moving in the xz plane [43,81,82], as presented in Fig. 3(b). As a result, the number of degrees of freedom in the system is significantly reduced.

It is assumed that the h-BN and G nanoribbons have the zigzag direction coinciding with the x axis (see Fig. 3), then the 2D chain model will describe the cross section of the multilayer system by the xz plane. One node of the 2D model represents all atoms of the nanoribbon having the same coordinates (x, z). In other words, the atoms located along the same line parallel to the y axis move synchronously, changing only the coordinates (x, z).

In the model under consideration, graphene sheets are not interconnected by covalent bonds, only weak van der Waalt forces act between them, so that the sheets can slide relative to each other.

The Hamiltonian of one h-BN (or G) nanoribbon has the form of the Hamiltonian of the chain of nodes moving in the xz plane:

$$H_i = \sum_{n=1}^{N} \left[\frac{1}{2} M_i(\dot{\mathbf{u}}_n, \dot{\mathbf{u}}_n) + V_i(R_n) + U_i(\theta_n) \right]. \tag{3}$$

Here the index $i = 1$ or 2 if h-BN or G nanoribbon is considered. The two-dimensional vector $\mathbf{u}_n = (x_n, z_n)$ defines the coordinates of the nth particle of the chain. The particle mass for the h-BN chain coincides with the average mass of the boron and nitrogen atoms $M_1 = M_{\mathrm{BN}} = (M_{\mathrm{B}} + M_{\mathrm{N}})/2 = 12.41 m_p$, and for the G chain it coincides with the mass of the carbon atom $M_2 = M_{\mathrm{C}} = 12 m_p$ ($m_p = 1.66 \cdot 10^{-27}$ kg is the proton mass).

The harmonic potential

$$V_i(R_n) = \tfrac{1}{2}\kappa_i (R_n - R_i)^2, \tag{4}$$

describes the longitudinal stiffness of the ith chain, where κ_i is the tensile stiffness of the bonds, $R_n = |\mathbf{u}_{n+1} - \mathbf{u}_n|$ is the length of the bond connecting the nodes n and $n + 1$, R_i is the equilibrium bond length of the ith chain.

The anharmonic potential

$$U_i(\theta_n) = \epsilon_i [1 + \cos(\theta_n)], \tag{5}$$

describes the bending stiffness of the ith chain, θ_n is the angle between two neighboring bonds, $\cos(\theta_n) = -(\mathbf{v}_{n-1}, \mathbf{v}_n)/R_{n-1}R_n$, vector $\mathbf{v}_n = \mathbf{u}_{n+1} - \mathbf{u}_n$.

The parameters of the potentials Eqs. (4) and (5) for the h-BN chain were determined in Ref. [83] and for the G chain in Refs. [81,82] from the analysis of the dispersion curves of the corresponding nanoribbons. For the h-BN chain stiffness is $\kappa_1 = 480$ N/m, pitch $R_1 = r_{\mathrm{BN}}\sqrt{3}/2 = 1.252$ Å ($r_{\mathrm{BN}} = 1.446$ Å is the length of B-N valence bond in h-BN sheet), and $\epsilon_1 = 1.10$ eV. For the G chain longitudinal stiffness is $\kappa_2 = 405$ N/m, chain pitch is $R_2 = r_{\mathrm{CC}}\sqrt{3}/2 = 1.228$ Å ($r_{\mathrm{CC}} = 1.418$ Å is the C-C valence bond length in graphene sheet), and $\epsilon_2 = 3.5$ eV.

Note that the Hamiltonian of the chain Eq. (3) gives the nanosheet deformation energy per longitudinal strip of width $\Delta y = \sqrt{3} R_i$. Further, the energy of the chains will be normalized by the graphene sheet width, so the energy of the h-BN sheets must be multiplied by the normalizing factor

$$c = \frac{R_2}{R_1} = \frac{r_{\mathrm{CC}}}{r_{\mathrm{BN}}} = 0.9808. \tag{6}$$

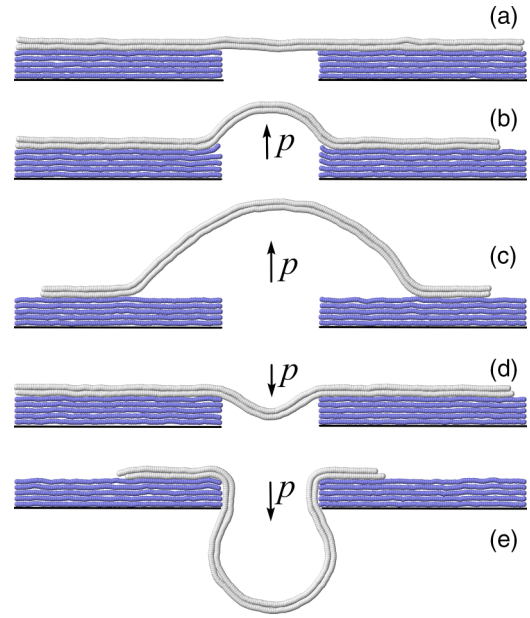

FIG. 4. Change in the shape of a bilayer graphene sheet under the action of pressure p (the arrow indicates the direction of the applied pressure): (a) the ground state of a multilayer system with a slit in the substrate at $p = 0$; (b) equilibrium profile of the G sheet at internal pressure $p = 0.96$ eV/nm^3; (c) postcritical behavior, i.e., formation of a rapidly growing bubble under the internal pressure $p = 1.26$ eV/nm^3, the G-sheet is detached from the substrate; (d) equilibrium sheet profile at external pressure $p = 1.34$ eV/nm^3; (e) postcritical behavior, i.e., fast pulling of the G sheet through the slit in the substrate at external pressure $p = 1.72$ eV/nm^3. The number of h-BN layers is $K_1 = 5$, the number of G layers is $K_2 = 2$, the number of chain nodes is $N_{\mathrm{BN}} = 100$ and $N_{\mathrm{C}} = 250$, width of the slit in the substrate is $d = 6$ nm, temperature $T = 300$ K.

The nonvalent interactions of nodes in chains and between chains are described with high accuracy by the (5,11) Lennard-Jones potentials

$$W_i(r) = \varepsilon_i [5(r_i/r)^{11} - 11(r_i/r)^5]/6. \tag{7}$$

Here r is the distance between the interacting nodes, ε_i is the interaction energy, r_i is the equilibrium bond length. Interactions of three types are considered: $i = 1$ is the interaction of the nodes of the h-BN chains, $i = 2$ is the interaction of the nodes of the G chains, and $i = 3$ is the interaction of the nodes of the h-BN chain with the nodes of the G chain. Parameters of the potential Eq. (7) are: $\varepsilon_1 = 0.01511$ eV, $r_1 = 3.642$ Å; $\varepsilon_2 = 0.0083$ eV [83], $r_2 = 3.61$ Å [43]; $\varepsilon_3 = \sqrt{\varepsilon_1 \varepsilon_2} = 0.01120$ eV, $r_3 = (r_1 + r_2)/2 = 3.626$ Å.

When modeling the dynamics of a multilayer substrate, it is necessary to limit the number of layers. Therefore, we assume that the first (lowest) layer interacts with a stationary flat surface of the crystal (this surface is shown in Figs. 3 and 4 by a black line). The interaction energy of nodes with a fixed substrate can be described by the (k, l) Lennard-Jones

potential

$$P(h) = e_0[k(h_0/h)^l - l(h_0/h)^k]/(l-k), \tag{8}$$

where h is the distance of the node to the plane of the fixed substrate, e_0 is the interaction energy (adhesion energy), h_0 is the equilibrium length, powers $l = 10$ and $k = 3.75$ are used. For an h-BN sheet lying on a flat surface of an h-BN crystal we set $e_0 = 0.0974$ eV, $h_0 = 3.49$ Å [43].

Consider the structure of $K = 2K_1 + K_2$ layers shown in Fig. 3. Let the first $2K_1$ layers correspond to h-BN chains consisting of $N_k = N_{\rm BN}$ nodes, $k = 1, \ldots, 2K_1$. These layers lie on a flat solid substrate and interact with it and have a vertical slit of width d between them. We assume that the surface of the solid substrate coincides with the $z = 0$ plane. The last K_2 layers consisting of $N_k = N_{\rm C}$ nodes, $k = 2K_1 + 1, \ldots, K$, correspond to the G chains lying on the h-BN multilayer substrate and covering the slit. The coordinates of nodes of such a system of K chains are given by the vectors

$$\{\mathbf{u}_{n,k} = (x_{n,k}, z_{n,k})\}_{n=1,k=1}^{N_k,K},$$

where n is the node number of the kth chain, N_k is the number of nodes in the kth chain.

The Hamiltonian of the chain system has the form

$$H = \sum_{j=1}^{2K_1}\sum_{n=1}^{N_{\rm BN}} \frac{c}{2} M_1(\dot{\mathbf{u}}_{n,j}, \dot{\mathbf{u}}_{n,j}) + \sum_{j=2K_1+1}^{K}\sum_{n=1}^{N_{\rm C}} \frac{1}{2} M_2(\dot{\mathbf{u}}_{n,j}, \dot{\mathbf{u}}_{n,j}) + E_1 + E_2 + E_3, \tag{9}$$

where the first two terms give the kinetic energy of the h-BN and G chains, respectively, and the potential energy of the h-BN chains is

$$E_1 = c\sum_{j=1}^{2K_1}\sum_{n=1}^{N_{\rm BN}}[V_1(R_{n,j}) + U_1(\theta_{n,j}) + P(z_{n,j})] + c\sum_{i=1}^{2K_1-1}\sum_{j=i+1}^{2K_1}\sum_{n=1}^{N_{\rm BN}}\sum_{k=1}^{N_{\rm BN}} W_1(r_{n,i;k,j}), \tag{10}$$

the potential energy of the G chains is

$$E_2 = \sum_{j=2K_1+1}^{K}\sum_{n=1}^{N_{\rm C}}[V_2(R_{n,j}) + U_2(\theta_{n,j})] + \sum_{i=2K_1+1}^{K-1}\sum_{j=i+1}^{K}\sum_{n=1}^{N_{\rm C}}\sum_{k=1}^{N_{\rm C}} W_2(r_{n,i;k,j}), \tag{11}$$

the potential energy of interaction of h-BN chains with G chains is

$$E_3 = \sum_{j=1}^{2K_1}\sum_{i=2K_1+1}^{K}\sum_{n=1}^{N_{\rm BN}}\sum_{k=1}^{N_{\rm C}} W_3(r_{n,j;k,i}), \tag{12}$$

distance $r_{n,j;k,i} = |\mathbf{u}_{n,j} - \mathbf{u}_{k,i}|$.

The chain model has been successfully used to simulate properties of scrolls [81] and folds [82] of graphene nanoribbons, surface ripplocations [43], equilibrium structures [84,85], negative thermal expansion [86], partial auxeticity [87], and nonlinear excitations [88,89] of carbon nanotube bundles.

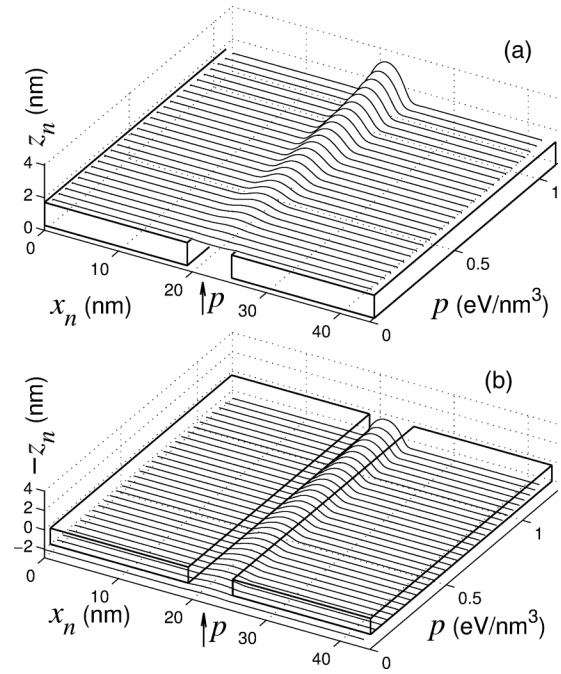

FIG. 5. Change in the stationary shape of a single-layer graphene sheet lying on a h-BN substrate with a slit of width $d = 6$ nm under the action of (a) internal and (b) external pressure (the arrow indicates the direction of the pressure p). Note that in (b) the ordinate has sign opposite to the sign in (a), i.e., the structure is shown upside down. The dependence of the shape of the cross section of the sheet on the pressure p can be seen. Number of layers is $K_1 = 5$, $K_2 = 1$, number of links in chains is $N_{\rm BN} = 150$, $N_{\rm C} = 352$. The maximum pressure value at which the sheet can withstand the pressures is (a) $p_0 = 1.03$ and (b) $p_0 = 1.19$ eV/nm^3. Temperature $T = 0$.

C. Potential energy minimization

To find the ground state of a multilayer system with a slit of width d in the substrate (see Fig. 5), it is necessary to numerically find the potential energy minimum

$$E = E_1 + E_2 + E_3 \to \min : \{\mathbf{u}_{n,j}\}_{n=1,j=1}^{N_j,\,K}, \tag{13}$$

with the initial position of its nodes

$$\begin{aligned} x_{n,k} &= (n-1)R_1, \quad z_{n,k} = kh_0, \\ x_{n,K_1+k} &= a_1 + (n-1)R_1, \quad z_{n,K_1+k} = kh_0, \\ k &= 1, \ldots, K_1, \quad n = 1, \ldots, N_{\rm BN}, \\ x_{n,2K_1+k} &= a_2 + (n-1)R_2, \quad z_{n,2K_1+k} = (K_1+k)h_0, \\ k &= 1, \ldots, K_2, \quad n = 1, \ldots, N_{\rm C}, \end{aligned} \tag{14}$$

where the shifts of the chains are $a_1 = (N_{\rm BN} - 1)R_2 + d$, $a_2 = [2(N_{\rm BN} - 1)R_1 + d - (N_{\rm C} - 1)R_2]/2$, $N_{\rm C} = [2(N_{\rm BN} - 1)R_1 + d]/R_2$.

To fix the size of the slit in the substrate, when solving the problem Eq. (13), the x coordinates of the edges of the substrate chains $x_{1,k}$ and $x_{N_{\rm BN},K_1+k}$, $k = 1, \ldots, K_1$, should be fixed. The problem Eq. (13) was solved numerically by the conjugate gradient method.

D. Accounting for the effect of temperature

Next, the multilayer system in the ground state is placed in a Langevin thermostat and its dynamics is considered. To do this, we numerically integrate the system of Langevin equations

$$M_k \ddot{\mathbf{u}}_{n,k} = -\frac{\partial H}{\partial \mathbf{u}_{n,k}} - \Gamma M_{n,k} \dot{\mathbf{u}}_{n,k} + \Xi_{n,k}, \quad n = 1, \ldots, N_k, \quad k = 1, \ldots, K, \tag{15}$$

where for chains $k = 1, \ldots, 2K_1$ the mass is $M_k = cM_{\mathrm{BN}}$, the number of nodes is $N_k = N_{\mathrm{BN}}$, for chains $k = 2K_1 + 1, \ldots, K$, $M_k = M_{\mathrm{C}}$ and $N_k = N_{\mathrm{C}}$. Here $\Gamma = 1/t_r$ is the friction coefficient characterizing the intensity of energy exchange with the thermostat (relaxation time is $t_r = 1$ ps), $\Xi_{n,k} = \{\xi_{n,k,i}\}_{i=1}^{2}$ is the two-dimensional vector of normally distributed random forces normalized by the conditions

$$\langle \xi_{n_1,k_1,i}(t_1) \xi_{n_2,k_2,j}(t_2) \rangle = 2\Gamma M_{n_1,k_1} k_B T \delta_{n_1 n_2} \delta_{k_1 k_2} \delta_{ij} \delta(t_2 - t_1),$$

here T is the thermostat temperature and k_B is the Boltzmann's constant.

In the numerical simulation of the dynamics for the substrate chains, we will use the conditions of fixed outer ends of h-BN chains (the ends that do not go into the slit)

$$\dot{\mathbf{u}}_{1,k} \equiv 0, \quad \dot{\mathbf{u}}_{N_{\mathrm{BN}},K_1+k} \equiv 0, \quad k = 1, \ldots, K_1, \tag{16}$$

which ensure the stability of the slit in the substrate. Note that the G chains ($k = 2K_1 + 1, \ldots, K$) can freely slide over the substrate, break away from it, or enter the slit.

E. Effect of pressure

To simulate the influence of pressure on the dynamics of G chains, additional forces f are introduced, which act on the nodes of the outer layer of the system orthogonally to its surface. In fact, viscous friction exists between the graphene sheet and the substrate, and this friction plays an important role when modeling dynamically applied pressure. Since we study quasistatic loading (slow increase of applied pressure), viscous friction does not affect the critical pressure values. Two cases will be considered: internal pressure acting from the slit, which can lead to the separation of G chains from the substrate [see Figs. 4(b), 4(c)], and external pressure, acting from above, leading to pressing the G chains into the slit [see Figs. 4(d), 4(e)].

In the first case, for the nodes of the inner G chain $k = 2K_1 + 1$ not adjacent to the substrate (which are at a distance $r > 5$ Å from the nodes of the h-BN chain) the force $f\mathbf{w}_{n,k}$ is added, where the unit-normalized vector

$$\mathbf{w}_{n,k} = (z_{n+1,k} - z_{n-1,k}, x_{n-1,k} - x_{n+1,k})/|\mathbf{u}_{n+1,k} - \mathbf{u}_{n-1,k}|$$

defines a direction orthogonal to the chain at its node (n, k). The magnitude of the force f characterizes the value of the pressure $p = f/\sqrt{3}R_2^2$.

In the second case, for the nodes of the upper G chain $k = K$ and for the atoms of the h-BN chains $k = K_1, 2K_1$ not covered from above by the G chains, to the right side of the equations of motion Eq. (15) the force $-f\mathbf{w}_{n,k}$ is added.

III. SIMULATION RESULTS

After describing the ground state of a G sheet on an h-BN substrate under internal and external pressure, the effect of temperature is analyzed. Then the critical pressure p_0 that can be sealed with G sheets is calculated as a function of temperature and slit width d. If the length of the graphene sheet is only slightly larger than the width of the slit, the contact area between them is very small. In this case, there is a certain probability that the graphene sheet may lose contact with the substrate due to thermal fluctuations, even if the pressure is less than p_0. To avoid this limiting case, graphene sheets with a length much larger than the slit width are considered.

A. Ground state of the system

Let us first consider how the stationary state of G sheet depends on internal or external pressure. As mentioned above, the forces f are added to the right side of the system of equations of motion Eq. (15), which describe the action of pressure normal to the G sheet. The initial configuration is the ground state of the multilayer system, i.e., the solution of the minimum energy problem Eq. (13) at $f = 0$. The structure of the system is modeled for a gradual and quasistatically increasing pressure (increasing f) at $T = 0$ K.

Simulation showed that the action of internal pressure first leads to the appearance of a stationary bulge located above the slit in the substrate, see Fig. 5(a). As the pressure increases, the height of the bulge increases monotonically. The growth of the bulge occurs not due to the stretching of the rigid valence bonds, but due to the sliding of the G chains along the substrate in the direction of the slit. As in the 3D case, the graphene nanoribbon slides on the substrate freely, with almost zero traction force. When the critical value of pressure p_0 is reached, the stationary bent state of the G chains ceases to exist. At $p > p_0$, the pressure from the substrate slit leads to the formation of a rapidly growing in time bubble under the graphene sheet, which leads to the separation of the sheet from the substrate, see Figs. 4(c) and 6(b).

Under the action of external pressure, see Fig. 5(b), the G chains bend inside the slit (note that here the direction of the ordinate is reversed). With such a quasistatic bending of a graphene sheet, its length practically does not change; bending occurs due to the sliding of the ends of the sheet towards the slit. Equilibrium profiles of the graphene sheet are possible only at $p < p_0$, where p_0 is the critical pressure. For $p > p_0$, the graphene sheet is dynamically pressed into the slit, see Figs. 4(e) and 7(b). Postcritical sliding of the graphene sheet into the slit occurs due to the sliding of the edges of the sheet into the slit at practically unchanged length of the sheet.

The critical values of internal pressure ($p_0 = 1.03$ eV/nm^3) and external pressure ($p_0 = 1.19$ eV/nm^3) obtained with the chain model should be compared with the values found in full-atomic simulations, see Table I. The difference is 4.8% and 9.7% for the external and internal pressures, respectively.

B. Effect of simulation parameters on critical pressure

To determine the critical pressure, the kinetic energy of the system is monitored during the quasistatic pressure increase.

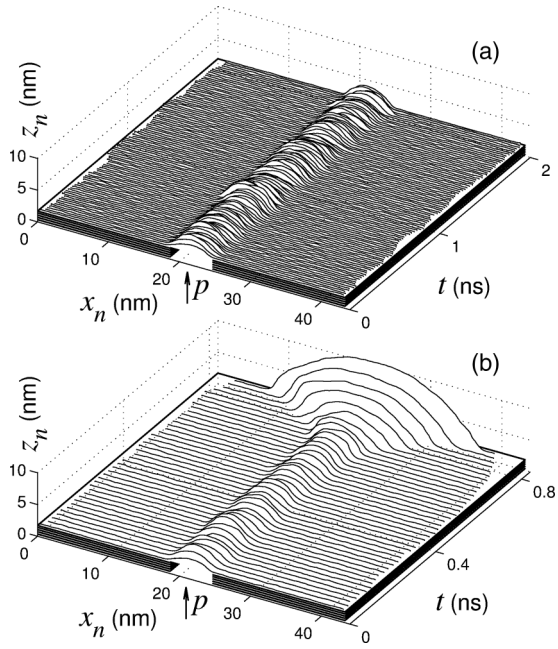

FIG. 6. The dependence of the sheet cross-sectional shape on time t for a single-layer graphene sheet under the action of internal pressure (shown by the arrow) at (a) $p = 0.766$ and (b) $p = 0.785$ eV/nm^3. Simulation temperature is $T = 300$ K, $K_1 = 5$, $K_2 = 1$, $N_{\rm BN} = 150$, $N_{\rm C} = 352$, and $d = 6$ nm. The critical pressure is $p_0 \approx 0.775$ eV/nm^3.

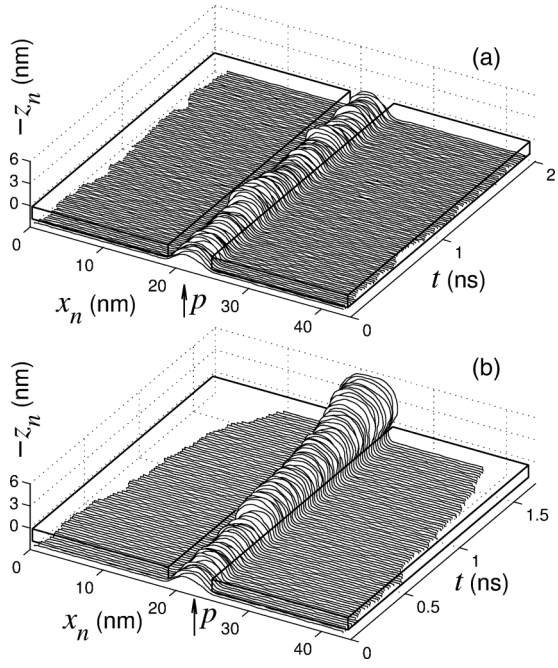

FIG. 7. The dependence of a single-layer graphene sheet cross section on time t under the action of external pressure (a) $p = 0.957$ and (b) $p = 0.995$ eV/nm^3. Note that $-z_n$ is used as the ordinate. Simulation temperature is $T = 300$ K, $K_1 = 5$, $K_2 = 1$, $N_{\rm BN} = 150$, $N_{\rm C} = 352$, and $d = 6$ nm. The critical value of pressure is $p_0 \approx 0.976$ eV/nm^3.

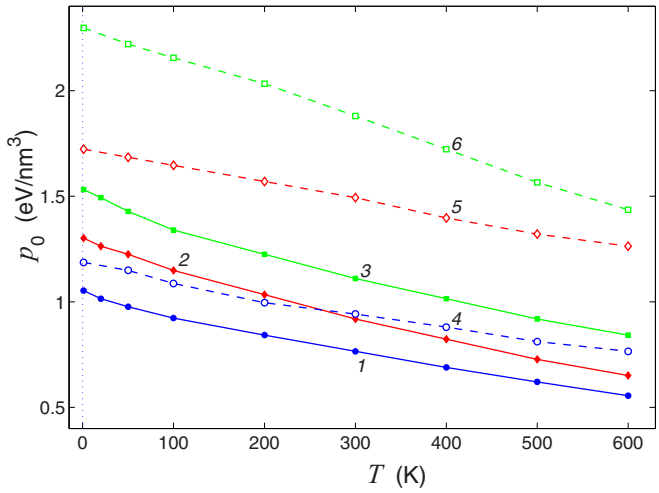

FIG. 8. Dependence of critical value of pressure p_0 on temperature T for internal and external pressure (solid and dashed curves, respectively). Curves 1 (4), 2 (5), and 3 (6) give the dependence for a single-layer, bilayer, and three-layer graphene sheet lying on a substrate with a slit of width $d = 6$ nm.

When the critical pressure is reached, the graphene sheet begins to deform dynamically, resulting in a large increase in the kinetic energy of the system. The critical pressure is defined as the pressure at which the quasistatic regime of sheet deformation changes to the dynamic regime, characterized by a sharp increase in kinetic energy.

The critical pressure p_0 depends on the temperature, the slit width, the number of graphene layers, and on the direction of the applied pressure (internal or external).

Modeling examples for $T = 300$ K are shown in Figs. 6 and 7 for constant internal and external pressures, respectively. Cases $p < p_0$ are shown in Figs. 6(a) and 7(a), and in Figs. 6(b) and 7(b) p exceeds a critical value. Relatively low pressure leads to the formation of a stable bulge of the G sheet at the slit, see Figs. 6(a) and 7(a). While pressure remains below the critical value, its increase leads only to an increase in the height of the bulge. When the critical value of internal pressure is reached, the stationary state of the G sheet becomes unstable and, under the action of pressure, a rapidly growing bubble is formed leading to the separation of the sheet from the substrate, see Fig. 6(b). Under the action of external pressure $p > p_0$, the G sheet is pushed into the slit of the substrate and a growing bubble is formed on its reverse side, see Fig. 7(b). The growth of the bubble in this case leads to the extrusion of the entire G sheet through the slit.

The dependence of the critical pressure on the number of nanoribbons in G sheet and temperature is given in Fig. 8. As can be seen, at any temperature, an increase in the number of graphene nanoribbons leads to an increase in the critical value of pressure p_0 because it leads to an increase in the flexural rigidity of the sheet, which leads to an increase in the resistance of the sheet to bending under pressure. But the main contribution to the pressure resistance comes from the energy of the interaction of the sheet with the substrate; it is this interaction that prevents the layer from being separated from

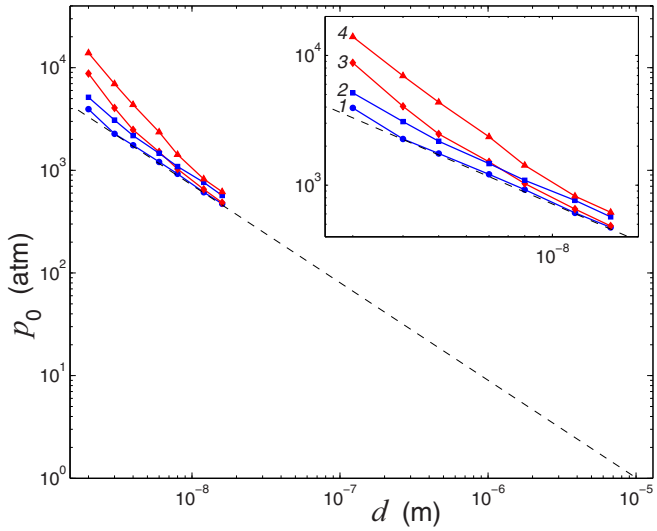

FIG. 9. Dependence of the critical value of pressure p_0 on the width of the slit in the substrate d for a single-layer (curves 1 and 3) and two-layer (curves 2 and 4) graphene sheet at internal (curves 1 and 2) and external (curves 3 and 4) pressure. The dashed straight line extrapolates the numerical data to atmospheric pressure. The equation of the line is $p_0 \approx 1.8\times10^{-5}/d^{0.95}$ atm. Temperature is $T = 300$ K.

the substrate. Thermal fluctuations lead to easier separation of the sheet from the substrate (there is an effective decrease in the interaction energy of one node with the substrate by k_BT), therefore, with increasing temperature, the critical pressure decreases almost linearly with temperature, see Fig. 8.

Numerical simulation showed that as the slit width in the substrate d increases, the critical pressure decreases as a power of the width: $p_0 \sim d^{-0.95}$, for $d \to \infty$, see Fig. 9. Note that for external pressure its critical value is always higher than that for internal pressure, but for $d > 10$ nm these values differ only slightly. Therefore, the resulting approximation of the dependence of the critical pressure on the slit width $p_0 \approx 1.8\times10^{-5}/d^{0.95}$ atm is valid for both internal and external pressures. This dependence allows one to conclude that at a temperature of $T = 300$ K, graphene sheets without their valence attachment to the substrate can effectively seal only cracks in the substrate with a width of $d < 1$ μm under excess pressure $p \sim 1$ atm.

IV. CONTINUUM MECHANICS TREATMENT

An understanding of the problem under consideration can be obtained with the help of membrane theory. In the case of $d \gg h$, where h is the thickness of the graphene sheet, the graphene sheet can be considered as an inextensible membrane, since the bending rigidity of graphene is much less than its tensile stiffness.

First we demonstrate that the graphene sheet partly lying on a substrate tends to slide onto the substrate and it can be in equilibrium only under the action of force F as shown in Fig. 10(a). Indeed, the energy of the van der Waals interaction between G and h-BN is proportional to the length L of the nanoribbon lying on the substrate,

$$U = eL, \tag{17}$$

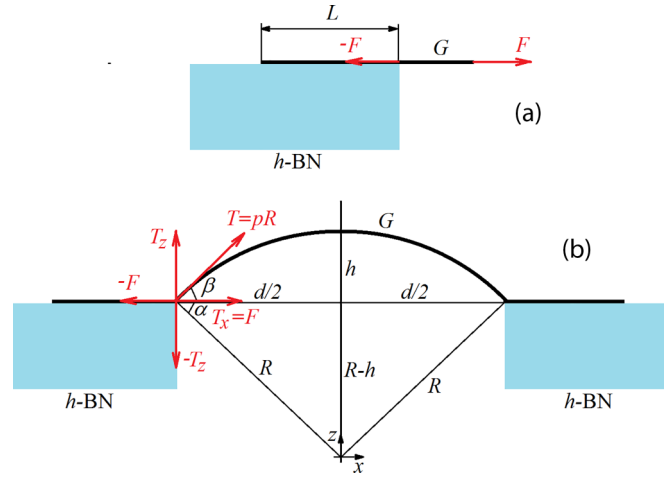

FIG. 10. (a) Scheme for calculating the force F pulling a graphene sheet onto the substrate. (b) Scheme of interaction forces between the graphene sheet under inner pressure and the substrate.

where e is the interaction energy per unit length. The force is

$$F = -\frac{dU}{dL} = -e. \tag{18}$$

The force F is constant, it depends only on the strength of van der Waals interactions and does not depend on the length L. The constancy of the shear cohesive force during peeling of a graphene sheet from a (111) Pt substrate was demonstrated in Ref. [61] using molecular dynamics.

The membrane under the action of internal pressure p acquires a cylindrical shape of radius R, see Fig. 10(b). The circumferential membrane force in the graphene sheet is

$$T = pR. \tag{19}$$

The friction between G and h-BN is negligible due to the incommensurability of the lattice pitch of G and h-BN, as well as thermal vibrations of the atoms depinning G from the substrate. Therefore, the graphene sheet is in the equilibrium due to the action of a tensile circumferential force $T = (T_x, T_z)$, and a force with components $(-F, -T_z)$, see Fig. 10(b). It is clear that $F = T_x$, and the force component $-T_z$ is due to the van der Waals coupling between G and h-BN.

It can be seen from Fig. 10(b) that

$$\cos\alpha = \frac{d}{2R}, \quad \cos\beta = \frac{F}{T}, \quad \beta = \frac{\pi}{2} - \alpha, \tag{20}$$

and hence

$$\frac{R}{d} = \frac{1}{2\cos\left[\arcsin\frac{F}{T}\right]}. \tag{21}$$

It is convenient to measure R and h in units of slit width d and the membrane forces in units of F since d and F are constants. In other words, the ratio T/F can be regarded as the loading parameter of the system as it increases with increasing p. Equation (21) gives R/d in terms of T/F. It is also possible to express T_z/F and h/d in terms of this parameter,

$$\frac{T_z}{F} = \cos\alpha = \frac{T}{F}\frac{d}{2R}, \quad \frac{h}{d} = \frac{R}{d} - \sqrt{\left(\frac{R}{d}\right)^2 - \frac{1}{4}}. \tag{22}$$

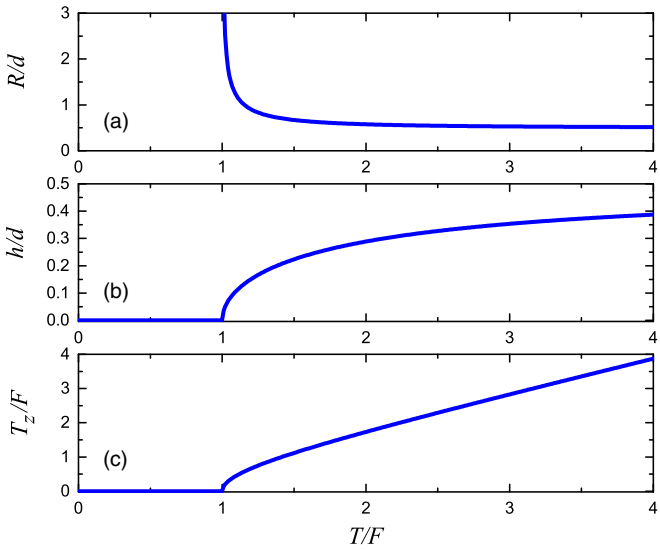

FIG. 11. As the functions of T/F shown are (a) R/d, (b) h/d, and (c) T_z/F.

In Figs. 11(a)–11(c) we present R/d, h/d, and T_z/F, respectively, as the functions of T/F. The curves are defined for $T/F \geqslant 1$ and $T/F < 1$ corresponds to the case of flat sheet ($R = \infty$, $h = 0$, and $T_z = 0$). Since the force F does not change when the graphene sheet is deformed by internal pressure, the sheet radius approaches the value $R = d/2$ from above, and h approaches the value $d/2$ from below. The radius of a cylindrical graphene sheet cannot reach the value $d/2$ (it corresponds to a half-cylinder), since in this case the membrane force T would have a zero component T_x, but this is possible only when the sheet is separated from the substrate, i.e. in the regime of postcritical blowup. As for the component T_z, for large values of T/F it increases proportionally to T, as follows from the first formula in Eq. (22) at $R \approx d/2$. An increase in this component will sooner or later lead to separation of the graphene sheet from the substrate.

The behavior of a graphene sheet under the action of internal pressure, observed in molecular dynamics simulations, agrees very well with the picture obtained in the framework of membrane theory. In particular, the thickness of the G sheet is not included in the equations describing the deformation of the membrane under pressure. This agrees with the results presented in Fig. 9, according to which the effect of the G sheet thickness is noticeable only for $d < 10$ nm and does not affect the critical pressure p_0 for large d. This is due to the fact that membrane theory assumes that the cylindrical part of the G sheet is connected to the flat part lying on the substrate without a transition zone, see Fig. 10. In fact, there is a smooth conjugation between these two parts of the G sheet, see Fig. 4, and the effect of this transition zone is noticeable only at small d.

V. CONCLUSIONS

The problem of finding critical pressure that a few-layer G sheet covering a slit of width d in h-BN substrate can withstand is considered using molecular dynamics simulation. First, the problem is approached using 3D atomistic modeling (see Sec. II A) and then the 3D problem is reduced to a 2D one, as shown in Fig. 3. The difference between the critical pressures calculated using 2D and 3D models is less than 10%.

In the case of $p < p_0$, where p_0 is the critical pressure, G sheet acquires an equilibrium curved profile, see Figs. 4(b), 4(d) and Fig. 5. At $p > p_0$, the equilibrium state of the G sheet becomes impossible, and under internal pressure it dynamically breaks away from the substrate, see Fig. 4(c), and under external pressure it is pressed into the slit, see Fig. 4(e).

The effect of the number of graphene sheets, temperature, and slit width on the critical pressure p_0 was analyzed. With an increase in the number of graphene sheets p_0 increases due to the increase in the bending stiffness of G sheet. However, this increase is only noticeable for very narrow slits $d < 10$ nm and for larger d the number of graphene sheets does not affect the critical pressure. This is because only a local area of the G sheet near the edge of the slit is strongly curved to ensure a smooth connection between the cylindrical and flat portions of the sheet. The curvature of the G sheet in this transition region depends on the thickness of the G sheet, but the influence of this region is noticeable only at small d. This conclusion is supported by the membrane theory, which predicts that the membrane thickness does not affect the critical pressure.

Increase of temperature leads to almost linear decrease in critical pressure, see Fig. 8. This is because the temperature effectively decreases the binding force between the G sheet and h-BN substrate.

The results obtained can be discussed in the light of theoretical works [53–55], in the sense of which type of loading (assigned force or assigned displacement) is realized in our simulation. According to the analysis presented in Ref. [54], for assigned displacement of the chain end, the force-extension curves have a maximum, and for assigned force, they increase monotonically. In our simulation, the detachment of the graphene sheet from the substrate occurs dynamically when the critical pressure value p_0 is reached, which is characteristic of loading by assigned displacement. It has also been shown that at a critical temperature the chain can detach from the substrate even with zero external force [53–55], but in our simulations we did not reach such a high temperature.

The critical pressure is nearly inverse proportional to the slit width, see Fig. 9, from which the approximation $p_0 \approx 1.8\times10^{-5}/d^{0.95}$ atm was extracted at a temperature of $T = 300$ K.

Figure 9 shows the extrapolation of the dependence $p_0(d)$ to a critical pressure of 1 atm. It can be seen that a pressure of 1 atm can be sealed with a G sheet if the slit width is $d < 10^{-5}$ m, i.e., less than 0.01 mm. For such a wide slit the number of graphene layers in the G sheet is not important.

ACKNOWLEDGMENT

Computational facilities were provided by the Interdepartmental Supercomputer Center of the Russian Academy of Sciences. This work was supported by the Russian Science Foundation, Grant No. 21-12-00229.

[1] K. S. Novoselov, A. K. Geim, S. V. Morozov, D. Jiang, Y. Zhang, S. V. Dubonos, I. V. Grigorieva, and A. A. Firsov, Science **306**, 666 (2004).

[2] A. H. Castro Neto, F. Guinea, N. M. R. Peres, K. S. Novoselov, and A. K. Geim, Rev. Mod. Phys. **81**, 109 (2009).

[3] E. Koren, I. Leven, E. Lörtscher, A. Knoll, O. Hod, and U. Duerig, Nat. Nanotechnol. **11**, 752 (2016).

[4] J. C. Meyer, A. K. Geim, M. I. Katsnelson, K. S. Novoselov, T. J. Booth, and S. Roth, Nature (London) **446**, 60 (2007).

[5] C. Lee, X. Wei, J. W. Kysar, and J. Hone, Science **321**, 385 (2008).

[6] A. Falin, Q. Cai, E. J. G. Santos, D. Scullion, D. Qian, R. Zhang, Z. Yang, S. Huang, K. Watanabe, T. Taniguchi, M. R. Barnett, Y. Chen, R. S. Ruoff, and L. H. Li, Nat. Commun. **8**, 15815 (2017).

[7] E. Han, J. Yu, E. Annevelink, J. Son, D. A. Kang, K. Watanabe, T. Taniguchi, E. Ertekin, P. Y. Huang, and A. M. van der Zande, Nat. Mater. **19**, 305 (2020).

[8] A. Zandiatashbar, G.-H. Lee, S. J. An, S. Lee, N. Mathew, M. Terrones, T. Hayashi, C. R. Picu, J. Hone, and N. Koratkar, Nat. Commun. **5**, 3186 (2014).

[9] I. A. Ovid'ko, Rev. Adv. Mater. Sci. **34**, 1 (2013).

[10] K. Cao, S. Feng, Y. Han, L. Gao, T. Hue Ly, Z. Xu, and Y. Lu, Nat. Commun. **11**, 284 (2020).

[11] I. V. Kosarev, S. V. Dmitriev, A. S. Semenov, and E. A. Korznikova, Materials **15**, 5900 (2022).

[12] E. Ganz, A. B. Ganz, L.-M. Yang, and M. Dornfeld, Phys. Chem. Chem. Phys. **19**, 3756 (2017).

[13] R. Ramírez, E. Chacón, and C. P. Herrero, Phys. Rev. B **93**, 235419 (2016).

[14] C. P. Herrero and R. Ramírez, Phys. Rev. B **97**, 195433 (2018).

[15] C. P. Herrero and R. Ramírez, J. Chem. Phys. **148**, 102302 (2018).

[16] F. Bonaccorso, L. Colombo, G. Yu, M. Stoller, V. Tozzini, A. C. Ferrari, R. S. Ruoff, and V. Pellegrini, Science **347**, 1246501 (2015).

[17] H. Fei, J. Dong, D. Chen, T. Hu, X. Duan, I. Shakir, Y. Huang, and X. Duan, Chem. Soc. Rev. **48**, 5207 (2019).

[18] S. Gupta and N.-H. Tai, Carbon **152**, 159 (2019).

[19] J. Kim, J. Jeong, N. Kim, R. Joshi, and G.-H. Lee, J. Phys. D **52**, 083001 (2019).

[20] F. Zhu, J. Leng, J.-W. Jiang, T. Chang, T. Zhang, and H. Gao, J. Mech. Phys. Solids **163**, 104871 (2022).

[21] Z. Huang, Z. He, Y. Zhu, and H. Wu, J. Mech. Phys. Solids **171**, 105144 (2023).

[22] I. Leven, D. Krepel, O. Shemesh, and O. Hod, J. Phys. Chem. Lett. **4**, 115 (2013).

[23] A. K. Geim and I. V. Grigorieva, Nature (London) **499**, 419 (2013).

[24] K. S. Novoselov, A. Mishchenko, A. Carvalho, and A. H. Castro Neto, Science **353**, aac9439 (2016).

[25] Z. Dai, N. Lu, K. Liechti, and R. Huang, Curr. Opin. Solid State Mater. Sci. **24**, 100837 (2020).

[26] C. R. Woods, L. Britnell, A. Eckmann, R. S. Ma, J. C. Lu, H. M. Guo, X. Lin, G. L. Yu, Y. Cao, R. V. Gorbachev, A. V. Kretinin, J. Park, L. A. Ponomarenko, M. I. Katsnelson, Y. N. Gornostyrev, K. Watanabe, T. Taniguchi, C. Casiraghi, H.-J. Gao, A. K. Geim *et al.*, Nat. Phys. **10**, 451 (2014).

[27] G. J. Slotman, M. M. van Wijk, P.-L. Zhao, A. Fasolino, M. I. Katsnelson, and S. Yuan, Phys. Rev. Lett. **115**, 186801 (2015).

[28] Y. Guo, X. Zhou, K. Lee, H. Yoon, Q. Xu, and D. Wang, Nanotechnol. **32**, 312002 (2021).

[29] A. Savin, Phys. Rev. B **106**, 205410 (2022).

[30] D. Mandelli, I. Leven, O. Hod, and M. Urbakh, Sci. Rep. **7**, 10851 (2017).

[31] C. R. Dean, A. F. Young, I. Meric, C. Lee, L. Wang, S. Sorgenfrei, K. Watanabe, T. Taniguchi, P. Kim, K. L. Shepard, and J. Hone, Nat. Nanotechnol. **5**, 722 (2010).

[32] W. Yang, G. Chen, Z. Shi, C.-C. Liu, L. Zhang, G. Xie, M. Cheng, D. Wang, R. Yang, D. Shi, K. Watanabe, T. Taniguchi, Y. Yao, Y. Zhang, and G. Zhang, Nat. Mater. **12**, 792 (2013).

[33] R. Kumar, S. Sahoo, E. Joanni, R. K. Singh, R. M. Yadav, R. K. Verma, D. P. Singh, W. K. Tan, A. Pérez del Pino, S. A. Moshkalev, and A. Matsuda, Nano Res. **12**, 2655 (2019).

[34] A. Kochaev, K. Katin, M. Maslov, and S. Singh, Phys. Rev. B **105**, 235444 (2022).

[35] A. A. Vasiliev and I. S. Pavlov, Mech. Res. Commun. **115**, 103732 (2021).

[36] V. I. Erofeev and I. S. Pavlov, Adv. Struct. Mater. **144**, 1 (2021).

[37] V. I. Erofeev, I. S. Pavlov, A. V. Porubov, and A. A. Vasiliev, Adv. Struct. Mater. **90**, 101 (2018).

[38] L. K. Galiakhmetova, I. S. Pavlov, A. M. Bayazitov, I. V. Kosarev, and S. V. Dmitriev, Materials **15**, 4871 (2022).

[39] J. G. McHugh, P. Mouratidis, and K. Jolley, Phys. Rev. B **103**, 195436 (2021).

[40] Y. Chen, L. Huang, C. Hu, T. Dumitrică, and H. Xu, Appl. Surf. Sci. **613**, 155979 (2023).

[41] F. Pan, G. Wang, L. Liu, Y. Chen, Z. Zhang, and X. Shi, J. Mech. Phys. Solids **122**, 340 (2019).

[42] M. Li, P.-F. Xu, J.-X. Shi, and X.-W. Lei, Comput. Mater. Sci. **224**, 112180 (2023).

[43] A. V. Savin, E. A. Korznikova, and S. V. Dmitriev, Phys. Rev. B **99**, 235411 (2019).

[44] J. Yu, S. Kim, E. Ertekin, and A. Van Der Zande, ACS Appl. Mater. Interfaces **12**, 10801 (2020).

[45] J. Williams, Int. J. Fract. **87**, 265 (1997).

[46] S. Koenig, N. Boddeti, M. Dunn, and J. Bunch, Nat. Nanotechnol. **6**, 543 (2011).

[47] X. Ma, L. Liu, Z. Zhang, and Y. Wei, J. Appl. Mech. T. ASME **89**, 031011 (2022).

[48] Y. Chen, W. Ouyang, K. Zhou, H. Qin, and Y. Liu, Extreme Mech. Lett. **52**, 101612 (2022).

[49] W. Wang, X. Ma, Z. Dai, S. Zhang, Y. Hou, G. Wang, Q. Li, Z. Zhang, Y. Wei, and L. Liu, Adv. Mater. Interfaces **9**, 2101939 (2022).

[50] Z. Cheng, H. Zhang, S. Le, H. Abuzaid, G. Li, L. Cao, A. Davydov, A. Franklin, and C. Richter, ACS Nano **16**, 5316 (2022).

[51] I. Kosarev, A. Kistanov, R. Babicheva, E. Korznikova, J. Baimova, and S. Dmitriev, Europhys. Lett. **141**, 66001 (2023).

[52] A. V. Savin and S. V. Dmitriev, Physica E **151**, 115735 (2023).

[53] A. Cannizzo, G. Florio, G. Puglisi, and S. Giordano, J. Phys. A: Math. Theor. **54**, 445001 (2021).

[54] G. Florio, G. Puglisi, and S. Giordano, Phys. Rev. Res. **2**, 033227 (2020).

[55] A. Cannizzo and S. Giordano, Phys. Rev. E **107**, 035001 (2023).

[56] J. Molina, J. E. Escobar, D. Ramos, E. Gil-Santos, J. J. Ruz, J. Tamayo, A. San Paulo, and M. Calleja, Nano Lett. **21**, 6617 (2021).

[57] K. Eom, H. S. Park, D. S. Yoon, and T. Kwon, Phys. Rep. **503**, 115 (2011).
[58] B. Xu, P. Zhang, J. Zhu, Z. Liu, A. Eichler, X.-Q. Zheng, J. Lee, A. Dash, S. More, S. Wu, Y. Wang, H. Jia, A. Naik, A. Bachtold, R. Yang, P. X.-L. Feng, and Z. Wang, ACS Nano **16**, 15545 (2022).
[59] J. Zhang, P. Chen, J. Peng, and Y. Zhang, Front. Mech. Eng. **8**, 912134 (2022).
[60] Z. Budrikis and S. Zapperi, Nano Lett. **16**, 387 (2016).
[61] Z. Guo, T. Chang, X. Guo, and H. Gao, Sci. Rep. **7**, 159 (2017).
[62] Z. Dai and N. Lu, J. Mech. Phys. Solids **149**, 104320 (2021).
[63] W. Deng and H. Kesari, J. Mech. Phys. Solids **148**, 104270 (2021).
[64] Z. Xue, G. Chen, C. Wang, and R. Huang, J. Mech. Phys. Solids **158**, 104698 (2022).
[65] A. L. Kitt, Z. Qi, S. Rémi, H. S. Park, A. K. Swan, and B. B. Goldberg, Nano Lett. **13**, 2605 (2013).
[66] Y. Rao, S. Qiao, Z. Dai, and N. Lu, J. Mech. Phys. Solids **151**, 104399 (2021).
[67] J. S. Bunch, S. S. Verbridge, J. S. Alden, A. M. Van Der Zande, J. M. Parpia, H. G. Craighead, and P. L. McEuen, Nano Lett. **8**, 2458 (2008).
[68] P. R. Kidambi, P. Chaturvedi, and N. K. Moehring, Science **374**, eabd7687 (2021).
[69] S. P. Koenig, L. Wang, J. Pellegrino, and J. S. Bunch, Nat. Nanotechnol. **7**, 728 (2012).
[70] P. Z. Sun, Q. Yang, W. J. Kuang, Y. V. Stebunov, W. Q. Xiong, J. Yu, R. R. Nair, M. I. Katsnelson, S. J. Yuan, I. V. Grigorieva, M. Lozada-Hidalgo, F. C. Wang, and A. K. Geim, Nature (London) **579**, 229 (2020).
[71] L. Wang, L. W. Drahushuk, L. Cantley, S. P. Koenig, X. Liu, J. Pellegrino, M. S. Strano, and J. Scott Bunch, Nat. Nanotechnol. **10**, 785 (2015).
[72] P. Z. Sun, M. Yagmurcukardes, R. Zhang, W. J. Kuang, M. Lozada-Hidalgo, B. L. Liu, H.-M. Cheng, F. C. Wang, F. M. Peeters, I. V. Grigorieva, and A. K. Geim, Nat. Commun. **12**, 7170 (2021).
[73] Z. Yuan, G. He, S. X. Li, R. P. Misra, M. S. Strano, and D. Blankschtein, Adv. Mater. **34**, 2201472 (2022).
[74] S. Zhang, N. Wu, Z. Zeng, R. Song, X. Han, X. Chen, D. Hou, A. Yao, and L. Wang, Cell Rep. Phys. Sci. **3**, 100947 (2022).
[75] A. V. Savin, Y. S. Kivshar, and B. Hu, Phys. Rev. B **82**, 195422 (2010).
[76] A. K. Rappé, C. Casewit, K. S. Colwell, W. A. Goddard, and W. M. Skiff, J. Am. Chem. Soc. **114**, 10024 (1992).
[77] L. Verlet, Phys. Rev. **159**, 98 (1967).
[78] V. Sorkin and Y. Zhang, J. Mol. Model. **17**, 2825 (2011).
[79] Z. Song, Z. Xu, X. Huang, J.-Y. Kim, and Q.-S. Zheng, J. Appl. Mech. **80**, 040911 (2013).
[80] S. Das, D. Lahiri, D.-Y. Lee, A. Agarwal, and W. Choi, Carbon **59**, 121 (2013).
[81] A. V. Savin, E. A. Korznikova, and S. V. Dmitriev, Phys. Rev. B **92**, 035412 (2015).
[82] A. V. Savin, E. A. Korznikova, and S. V. Dmitriev, Phys. Solid State **57**, 2348 (2015).
[83] A. V. Savin, J. Exp. Theor. Phys. **133**, 754 (2021).
[84] L. Kh. Rysaeva, E. A. Korznikova, R. T. Murzaev, D. U. Abdullina, A. A. Kudreyko, J. A. Baimova, D. S. Lisovenko, and S. V. Dmitriev, Facta Univ. Ser.: Mech. Eng. **18**, 001 (2020).
[85] L. Kh. Rysaeva, D. V. Bachurin, R. T. Murzaev, D. U. Abdullina, E. A. Korznikova, R. R. Mulyukov, and S. V. Dmitriev, Facta Univ. Ser.: Mech. Eng. **18**, 525 (2020).
[86] L. K. Galiakhmetova, E. A. Korznikova, A. A. Kudreyko, and S. V. Dmitriev, Phys. Status Solidi-RRL **16**, 2100415 (2022).
[87] E. A. Korznikova, K. Zhou, L. K. Galiakhmetova, E. G. Soboleva, A. A. Kudreyko, and S. V. Dmitriev, Phys. Status Solidi-RRL **16**, 2100189 (2022).
[88] L. K. Galiakhmetova, D. V. Bachurin, E. A. Korznikova, A. M. Bayazitov, A. A. Kudreyko, and S. V. Dmitriev, Mech. Mater. **174**, 104460 (2022).
[89] A. V. Savin, E. A. Korznikova, and S. V. Dmitriev, J. Sound Vib. **520**, 116627 (2022).